

Research Article

Large-Time-Step-Based Ray-Tracing Modeling of Light Delivery in One-Sidedly Cladding-Removed Step-Index Plastic Optical Fiber under Arbitrary Weave Structure

Sun Hee Moon and In Hwan Sul 

Department of Materials Design Engineering, Kumoh National Institute of Technology, Gumi 39177, Republic of Korea

Correspondence should be addressed to In Hwan Sul; inhwan.sul@gmail.com

Received 9 July 2018; Accepted 6 September 2018; Published 15 November 2018

Academic Editor: Lijing Wang

Copyright © 2018 Sun Hee Moon and In Hwan Sul. This is an open access article distributed under the Creative Commons Attribution License, which permits unrestricted use, distribution, and reproduction in any medium, provided the original work is properly cited.

An advanced theoretical method to simulate the light delivery in plastic optical fiber is presented. The final objective is to use “light” as a new media for information delivery in wearable computers. A large-time-step-based ray-tracing algorithm, which was improved from our previous research, was used to simulate the light vector movement in a complex weave structure efficiently. NURBS and free-form-deformation-based modeling was used to mimic the arbitrary weave structure. Experimentally, optical fibers were modified to control the direction of light emission. Particularly, half side of a cladding layer in the radial direction was selectively removed to enhance one-sided fabric light scattering. The cladding-removed plastic optical fiber was adopted in a textile weave structure, and its light scattering was measured quantitatively by varying the removal length, fiber curvature, and fabric weave patterns. To show the validity of the proposed simulation technique, twill structures with varying number of cross repeat numbers were used as a testbed. The unit number 2 was found to be the optimal structure for light emission, when a single POF was embedded in the textile. The proposed model showed the similar result with the actual light intensity measurement, with computation time not much than one second.

1. Introduction

A wearable computer is considered a typical exemplary product of the fourth industrial revolution. While conventional garments provide mere protection from environment to humans, the wearable computer has additional functionality of delivering information. Therefore, value creation is expected via the wearable computer industry.

Conducting fibers and electronic devices seem to be the mainstream components in wearable computer research and development in these days. However, they lack of “flexibility” and “safety,” which are crucial factors in garment. Alternatively, plastic optical fibers (POFs) can be a good candidate for flexible wearable computer component. It is much flexible than conventional glass optical fibers (GOFs) or copper wires. Also it can deliver information using “light” as a media, giving no harm to

human health. Light delivery in optical fibers, which is known as waveguide theory, was already established in the 70s. However, this paper presents a more convenient and computationally efficient method for light delivery modeling using ray-tracing algorithm.

Ray tracing was already used in our previous work [1] for a plain weave structure with a POF whose entire cladding was removed radially. The amount of light transferred was successfully measured both theoretically and experimentally. However, the methodology had some limitations. Light dissipated into both sides of the fabric, which is undesirable because light does not have to be delivered to the human skin side. Further, B-spline was used to control the fiber shape; however, the control points moved only in a sinusoidal shape, which could model only the basic plain weave structure. In addition, the light vectors were advanced only at a small time step, which was equivalent to the wavelength, at each frame,

and the total simulation needed considerable time. Moreover, there were several errors in the vector direction especially when the vector resided at the core/cladding or cladding/air interface.

The present study modifies the previous work [1] to deal with arbitrary weave structure more efficiently. The free-form deformation (FFD) technique was applied to control the shape of the fibers arbitrarily. It can input the fabric weave structure by a simple series of alphabets, and then the weave structure is reconstructed automatically in 3D. In addition, a large time step was used in the ray-tracing algorithm. Once the total length of the traveling light was given, its course was dissected repetitively based on the light-fiber collision detection information. Moreover, POF specimens were generated by eliminating the claddings selectively only in one direction to maximize light scattering. The lights delivered through the one-sidedly cladding-removed fibers were measured both experimentally and theoretically. To show the validity of the proposed method, twill structures with varying number of cross repeat numbers were used as testbed. Before explaining the actual methodology, literatures on wearable computers and optical fibers are presented briefly.

2. Literature Review

A wearable computer is composed of several parts such as sensors [2] that receive information from environment, conductive fibers or fabrics [3] that transmit the received information, central information processing unit with an operating system such as Arduino [4], and actuators [5] that respond back to the environment based on the processed information. Sensors and actuators are generally made of ceramic materials, which have high permittivity; however, the high bending stiffness of ceramic renders its application to wearable devices difficult. Meanwhile, conductive fibers are prepared by surface coating of conductive materials onto nonconductive polymeric fibers [6], or by in-situ polymerization [7]. However, most of the conductive materials, such as carbon nanotubes, have a low washing durability [8]. Typical garments should stand at least 30 washing cycles according to the AATCC standard [9]. Moreover, using electric conductivity can cause another problem, i.e., electric shock. Electric current higher than 10 mA (60 Hz, 1 s) can lead to muscle contraction, pain, or even heart attack [10].

The above-mentioned materials use “electricity” as information delivery media. Electricity as a medium has shown excellent performance in various areas. However, it has several problems such as washing durability or wearability with regard to garments. In this paper, we suggest another information delivery media, i.e., “light” [1]. Light-based communication technology such as optical fibers is already being used actively since the 1970s [11].

GOF is a well-known technology used for various telecommunication systems such as submarine cables or fiber-to-home high-speed Internet lines [12]. The biggest advantage of GOFs is that they can deliver multiple channels simultaneously via multiplexing using 1550 nm wavelength

[13] light, at which GOFs show the lowest attenuation. GOFs have a high bending stiffness, and thus, it is impractical to use them as subsidiary materials for garments. POF is more advantageous in this regard. They have a slightly higher level of attenuation than GOFs do at 1550 nm, but show lower attenuation under visible light. Particularly, the flexibility of POFs is an important factor when applied to wearable computers.

There has been extensive research on the theoretical modeling of light transfer in optical fibers since 1970s. The waveguide theory generally deals with a simple cross-sectional geometry such as a circle or rectangle because it is written in complex partial differential equations. In the real world, fabrics have a complex three-dimensional structure, and the conventional waveguide theory cannot be applied easily for such complex boundary conditions.

Woven fabrics are composed of warp and weft yarns. If the warp and weft yarns are seen one by one at the surface, the fabric is called as “plain weave.” If either of the yarns has more than two exposed surfaces in a diagonal pattern, the structure is called as “twill.” Finally, satin has minimum crossings of warp and weft yarns, which yield more shiny fabrics using specular reflection of fiber surfaces. These are the three basic structures of woven fabrics. Meanwhile, the use of Jacquard loom can generate arbitrary structures of fabric by controlling each warp thread individually [14]. A fiber’s longitudinal path and cross section is deformed once it is woven into a fabric. The path is changed into a sinusoidal or any other wavy pattern depending on the weave structure. Such wavy patterns are called as “crimp” in textile science [15]. In the meantime, the cross section of a fiber also changes because of interfiber friction and interaction. Thus, the conventional waveguide theory cannot be easily applied to POFs inside a weave structure. Therefore, our strategy is to apply a ray-tracing algorithm, which is used for scene rendering in the field of computer graphics to predict the light transfer behavior through optical fibers under an arbitrary weave structure.

3. Materials and Methods

3.1. POF Specimen. PMMA-based step-index POF (Toray, Raytela®) was chosen for the experiment (Tables 1 and 2). Fiber diameters were chosen considering the efficiency of the weaving process afterwards.

3.2. Cladding Removal. Both chemical and mechanical methods were applied to remove cladding partially and selectively. A 100% solution of dimethyl ketone (DMK or acetone; from Daejung Chemical Corp.) was prepared for chemical treatment. Half the side of a POF was immersed in the solution for 0.5 h and then water washed, while the other side was masked with a tape (Scotch Magic; 3M). For mechanical cladding-removal treatment, sandpaper (grit size P80; ISO/FEPA) was used with 10 abrasions for each specimen. The fibers after treatment were impregnated with epoxy resin, and their cross sections were then observed using a cryo-ultramicrotome (RMC/PTPC&CRX)

TABLE 1: Overall specification of POF specimens.

Type	Value
Core material	PMMA
Core refractive index	1.49
Clad material	Fluorinated polymer
Clad refractive index	1.41
Refractive index profile	Step index
Numerical aperture	0.50
Acceptance angle	60°
Service temperature	-55 to 70°C
Min. attenuation	<650 nm

TABLE 2: Detailed dimensions of three types of POF specimens.

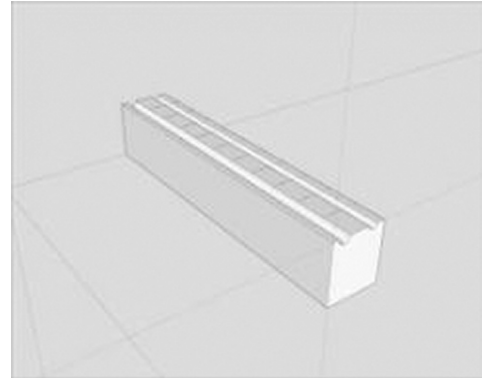
Name	Diameter (μm)	
	Core	Clad
PGR-FB250	240	250
PGR-FB750	735	750
PGR-FB1000	980	1,000

and a field-emission scanning electron microscope (JSM-6500F, JEOL).

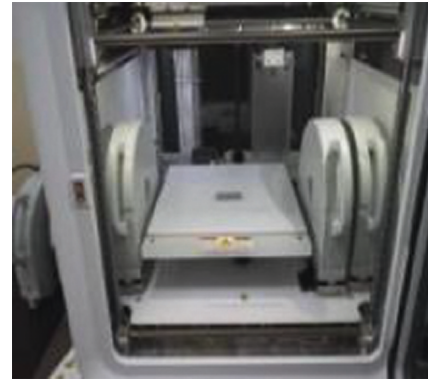
3.3. Light Source and Relative Intensity Measurement. A red LED (627 nm; Ocean Optics, Inc.) was used as a light source and connected at one end of a fiber. A USB-type flame spectrometer (FLAME-S-VIS-NIR, Ocean Optics corp.) was prepared and connected to the other end of the fiber to measure the “end-tip-illumination.” Another same spectrometer was connected to the cladding-removed site to measure “side-illumination.” A POF, the light source, and the spectrometers were interconnected using bare fiber adapters (BFA-KIT; Ocean Optics, Inc.) to minimize connection loss. Note that the intensities in the following graphs are shown as a relative normalized value because the LED strength could only be controlled manually by turning a jog dial. Every day, the initial light strength (I_0) was measured, and then the actual intensities (I_c) were divided by the initial value. Thus, the normalized values (I_c/I_0) were used to minimize a possible daily light intensity deviation.

3.4. Side-Illumination Measurement of POF. Before measuring light intensity of the POF inside the weave structure, the light intensity of a straight POF with no crimp was measured in advance. To keep the specimen straight, a simple jig was designed and printed using a 3D modeling tool (123D®, Autodesk; Figure 1(a)) and a 3D printer (Cube Trio Pro®, 3DSYSTEMS; Figure 1(b)).

For the POF inside the weave structure, both light scattering strength and area were measured quantitatively. For the former, a spectrometer for side-illumination measurement was used again. For the latter, an image analysis technique was used; the POF fabric was covered with a semitransparent rectangular acrylic plate in a dark room, and light was captured using a digital camera (A7K, Sony; Figure 2(a)). Then, the area from the light was



(a)



(b)

FIGURE 1: Jig 3D printing for light delivery measurement of unbent POF. (a) Jig design using Google SketchUp. (b) 3D-printed jig.

calculated using a thresholding operator in ImageJ software (Figures 2(b) and 2(c)).

3.5. POF-Textile Weaving. A small handloom (Loomini®; Luzium corp.) of 22.0 cm \times 32.5 cm size was used to prepare an arbitrary structure weave fabric. POF and wool/nylon combined yarn (70% : 30%; diameter: 3 mm) were used as a warp thread, while cotton/acrylic combined yarn (60% : 40%; diameter: 2 mm) was used as a weft thread. Diameters of the warp and weft yarns were chosen to the same with the POF specimen.

4. Modeling

4.1. Fiber Model. A fiber was assumed to be a discrete series of two cylinder sets with different radii (Figure 3(a)). The inner and outer cylinders correspond to a POF core and cladding, respectively. To mimic an actual woven fabric (Figure 3(b)), the positions of the cylinders were controlled by a “peg string” and “NURBS” (nonuniform rational B-spline) curve. Then, warp and weft information was input by either the “W” or “F” alphabet, also known as a peg string (Figure 3(c)). The undeformed cylinders’ central positions were aligned with the NURBS control point initially (Figure 3(d)). Then, the corresponding NURBS control point with respect to the given peg character was moved upward or downward (Figure 3(e)). The entire cylinder geometry was

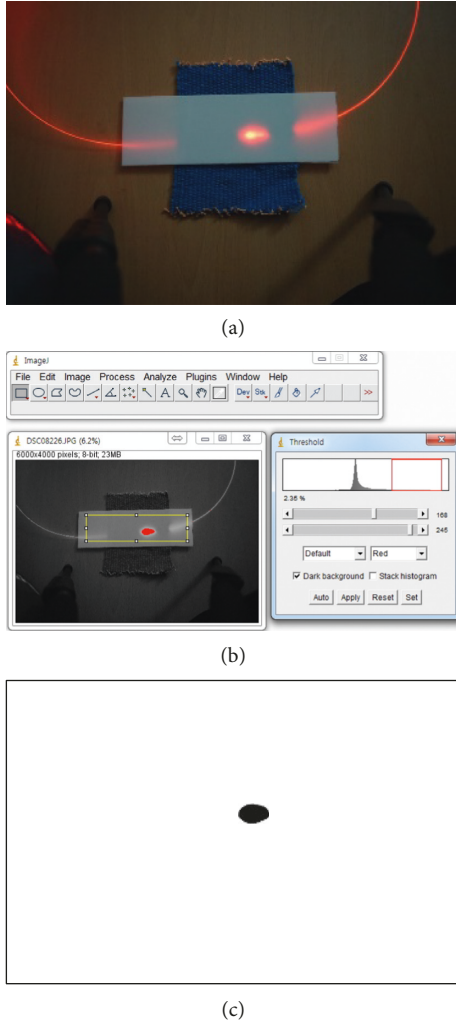


FIGURE 2: Measurement of total light scattered area using image analysis tool. (a) Example of an original image. (b) Image processing using ImageJ software. (c) Resultant thresholded image.

transformed following the NURBS movement using FFD (Figure 3(f)). In some areas including mechanics, “deformation” means change of shape resulted from external force. But it is far beyond the scope of this paper, to consider all the fiber-to-fiber interactions and predict the final crimp structure. Thus, the terminology, “deformation,” means only change of fiber crimp, without considering any external forces, throughout the paper. Figure 4 illustrates the modeling software developed in MS windows 7 environment using C++ language (C++ Builder XE5; Embarcadero Technologies, Inc.). The input fiber dimension values (Figure 4(c)) were matched to those of the actual commercial POF’s in Table 1. OpenGL 2.0 was used for rendering 3D objects on the screen.

4.2. Large-Step Ray-Tracing Algorithm. Our previous work [1] used a small-time-step-based ray-tracing strategy, in which light vectors advanced by the length of its wavelength

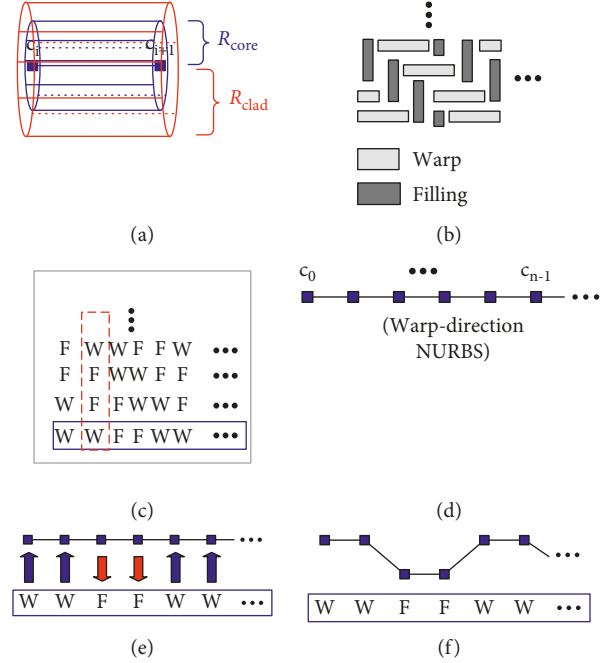


FIGURE 3: Procedure for weave structure modeling using NURBS. (a) Cylinder models for core and cladding representation [1]; (b) target fabric weave structure; (c) weave peg string input (dashed: weft, solid: warp direction); (d) initial NURBS control points (for warp); (e) adjustment of control points using peg string; (f) final crimp structure.

at each time frame. This resulted in redundant calculation (Figure 5) and several round-off errors especially at fiber interfaces. In the modified method, a very large length is provided for each light vector initially (\mathbf{v}_0 ; Figure 6(a)), and its collision sites with the core-cladding interface or cladding-air interface were determined ($\mathbf{q}_{c1} \sim \mathbf{q}_{c2}$; Figure 6(b)). Snell’s law was applied to the first collision site (\mathbf{q}_{c1} ; Figure 6(c)), and the initial vector (\mathbf{v}_0) was dissected into two parts: one before collision (\mathbf{v}_{c1}) and the other after collision. Depending on the refractive index distribution, the latter vector could be either refraction ($\mathbf{v}_{1c,rr}$; Figure 6(c)) or total internal reflection ($\mathbf{v}_{1c,ti}$; Figure 6(d)). The collision detection and Snell’s law were applied repetitively until there was no collision. The light intensity could be measured at any position of the POF by counting the number of light vectors (Figure 7).

5. Results and Discussion

5.1. Large-Time-Step-Based Ray-Tracing Modeling. Ray vector marching per frame inside an uncladded POF was successfully modeled, as shown in Figures 8(a)–8(e). Most of the ray vectors reached the terminal point, as shown in Figure 8(e). Figure 8(f) is an example of round-off error at the interfaces when a small time step was used. The use of a large time step minimized the number of collisions detected and Snell’s law application, which resulted in a more accurate ray-tracing result, as shown in Figure 8(e). The simulation speed was also drastically minimized (Table 3).

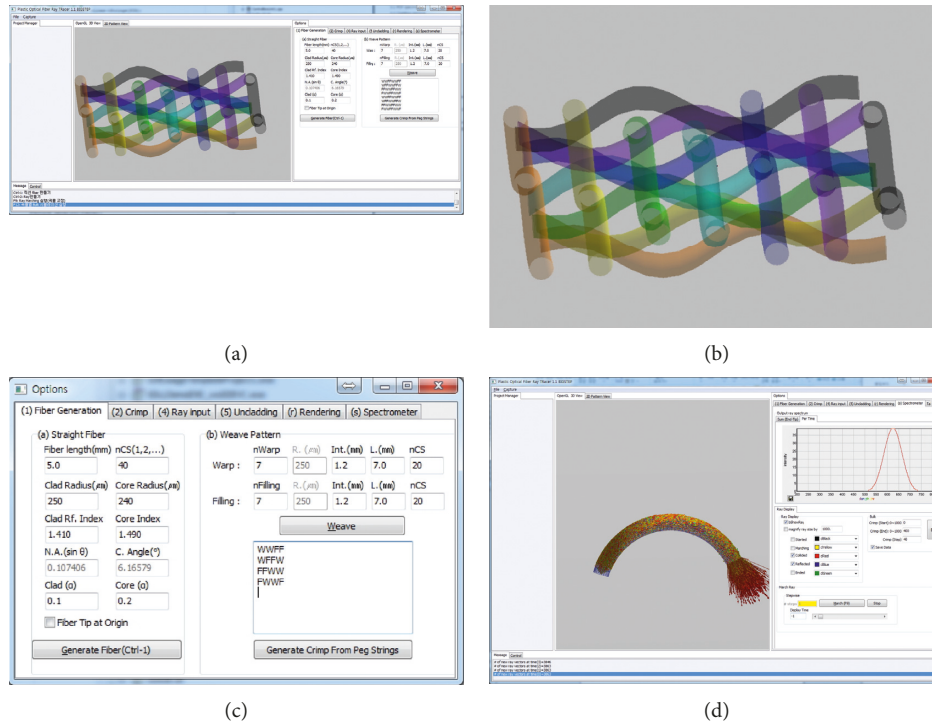


FIGURE 4: Fabric weave structure modeling result. (a) Program screenshot; (b) rendered view of 2 by 2 twill structure in detail; (c) fabric dimension and structure input window in detail; (d) theoretical light scattering measurement.

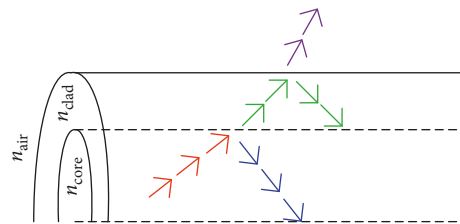


FIGURE 5: Schematic view of small-time-step-based ray-tracing [1] (vector size was exaggerated for display).

5.2. Comparison of Cladding Removal Methods. One-sided cladding removal of POF was verified. Especially, chemically cladding-removed surface (Figures 9(b) and 9(e)) had a different surface polishing from that of the untreated one (Figures 9(a) and 9(e)). Sandpaper method was also applied, but its effect was not uniform (Figures 9(c) and 9(f)). However, it was difficult to visually check whether the cladding was peeled off because the cladding had a relatively lower radius than the core did. Therefore, side illumination was measured in the radial direction at the cladding-removed surface. Figure 10 shows that one side (angle 0 radian) has higher intensity than the other side (3-4 radian).

The effect of one-sided cladding removal was compared with that of the whole-cut method (Figure 11). The intensity with zero cladding removal length is almost the same in the two methods (top-most solid line in Figures 11(a) and 11(b)). In addition, both the graphs show a decrease in intensity as the removal length increases. However, one-sided removal showed a more linear tendency, which implied that cladding operation was more regularly treated.

The end-tip-illumination with varying radius of curvature (designated as “ R_c ”) was measured for whole-cut and one-sided cladding-removed POFs, and the simulation result was added to the graph (Figure 12). Note that the x -axis of the graphs in Figure 12 was curvature, which was inversely proportional to radius. In our previous work [1], PGR-FB250, PGR-FB750, and especially PGR-FB1000 specimens showed an erroneous behavior. This implied that the bigger the radius, the greater is the difficulty in controlling the depth of cladding removal. However, the same tendency between experiment and simulation in Figure 12 shows that our new method can model the actual light delivery phenomena effectively. Yet, there was a constant gap between simulation and experiment. The gap may be easily calibrated by repeated experiments if needed, but we did not modify the result to show the pros and cons of our new method simultaneously.

5.3. Effect of Curvature on Light Delivery. Figure 13 shows the side-illumination from the cladding-removed POF, which is

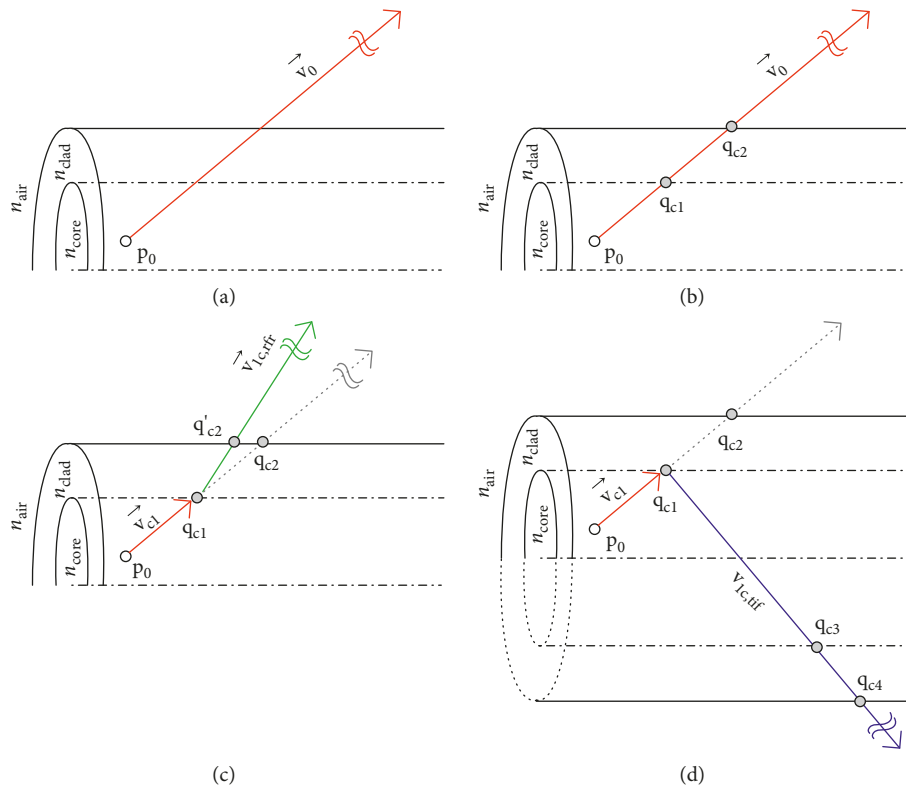


FIGURE 6: Diagram of the proposed large-time-step-based ray-tracing.

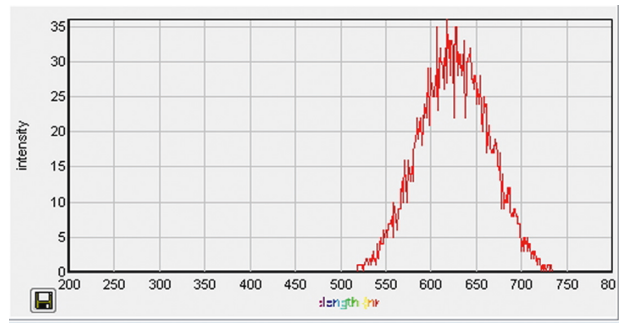


FIGURE 7: Screenshot of the light intensity measured using the proposed simulation technique.

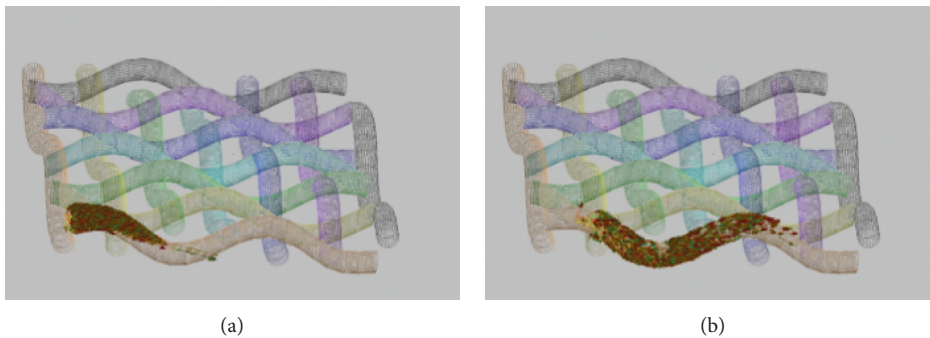


FIGURE 8: Continued.

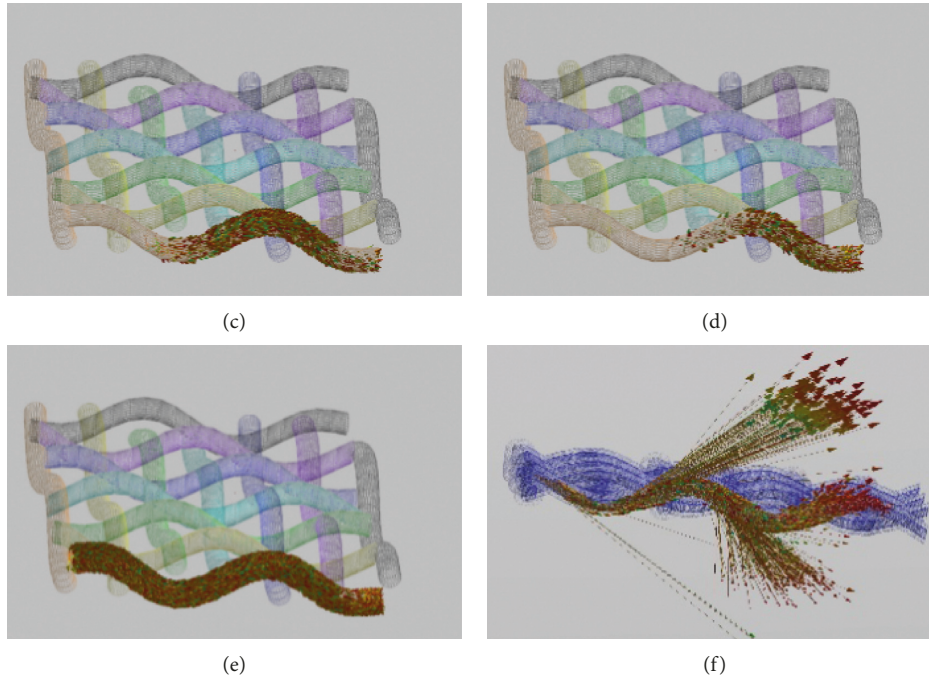


FIGURE 8: Progressive view of ray vector marching per frame inside uncladded POF. (a) Frame 1st. (b) Frame 4th. (c) Frame 7th. (d) Frame 10th. (e) All vectors. (f) Round-off error in small-step version.

TABLE 3: Simulation speed comparison between small-step and large-step models.

# of rays	Simulation time (min:sec.msec)	
	Small step	Large step
100	0:07.767	0:0.19
1009	1:25.208	0:0.780
2007	3:53.325	0:0.139
4015	7:42.042	0:0.247
8005	15:19.802	0:0.528

POF length = 5 mm; curvature = 0.571 mm^{-1} ; no. of cylinders for a fiber = 20; cladding not removed.

not yet inserted into the weave structure. As expected, the removal length showed a high linear tendency with the illumination area.

To verify the effect of curvature on POF light delivery, the cladding-removed POF with 1 cm uncladding length was given a series of curvature variations using the half-cone jig from our previous work [1] (Figure 14). The area of side-illumination showed a very high linearity with respect to the curvature (Figure 14, regression line $y = -892.9x + 49553.6$, $R^2 = 0.996$). Moreover, the relative intensity showed a similar result (Figure 15). These results revealed that more global bending generated a smaller area and higher intensity of side-illumination.

5.4. Application to Optimal Weave Structure Design. One-sided cladding removal and large-step-based ray-tracing techniques were verified for a single POF in the previous sections. The next goal was to show the validity of

our method by applying the proposed method by finding an optimal weave structure that maximizes the light delivery in cladding-removed POF. However, it is infeasible to check all the possible weave structures. Using Jacquard loom machine, there can be infinite number of weave configurations. Therefore, the testbed was limited to a satin structure, in which the number of crossed repeat units was used as an independent variable. It is quite possible to use multiple numbers of fibers, but only a single fiber was used for the sake of experimental simplicity. PGR-FB750 POF was again used as a specimen. The POF was inserted into the weave structure as one of the warp yarns, and then, its cladding was removed using acetone. For the simulation, cylinders of the cladding layer were also removed. Figure 16 shows the side-illumination area with different warp peg repeat number. For example, a cross repeat unit number “2” implies that the warp yarn is shown at the fabric surface twice in a series, and then, the weft is shown. Figure 16 does not have any meaningful extremal point, which indicated that a higher number of repeat units implies a greater possibility of exposing the warp yarn. However, Figure 17 shows a peak value of “2.” Although the number “2” has a lower value of illumination area in Figure 16, it has maximal value in the accumulated relative intensity. This phenomenon was observed in both the experiment and simulation. This can arise from two factors. First, it was verified that the curvature of a single POF increased the relative intensity (see Figure 15). However, there is a second factor called global bending. The POF inside the weave structure is given a series of different-sized crimps unlike the single crimp case shown in Figure 15. It is known that global bending is one of the attenuation factors in optical

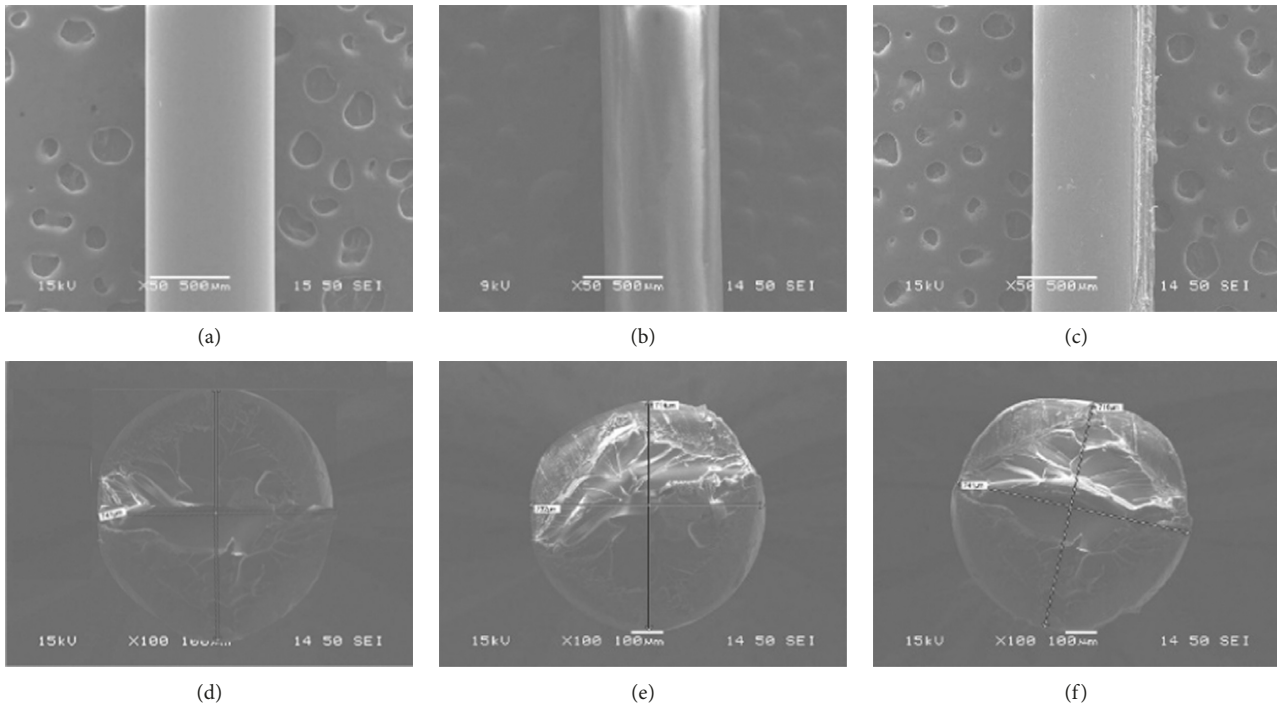


FIGURE 9: Result of half removal of cladding using chemical and mechanical methods. (a) Untreated fiber (PGR-FB750). (b) Half removal using acetone. (c) Half removal using sandpaper. (d) Untreated fiber (cross section). (e) Half removal using acetone (cross section). (f) Half removal using sandpaper (cross section).

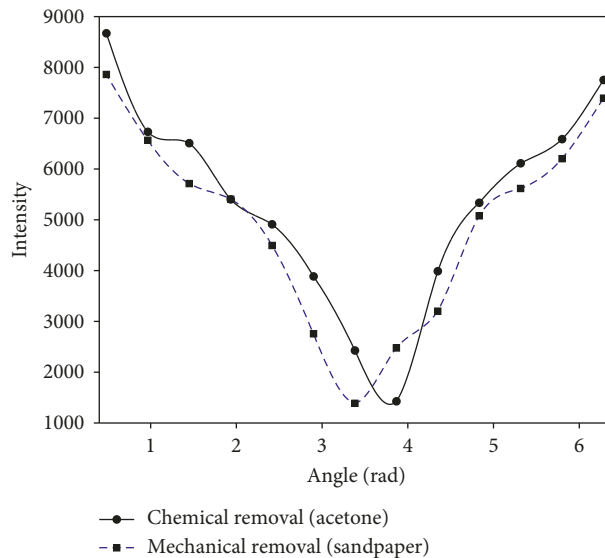


FIGURE 10: Radial distribution of maximum side-illumination of PGR-FB750 specimen after chemical and mechanical treatment.

fibers [13]. The increase in warp crossing led to an increase in global bending, which again resulted in a decrease in the relative light intensity. Thus, the maximal value at crossing number “2” seems to originate from the curvature effect and global bending effect. Using this fact, we manufactured a 2 by 2 twill fabric, in which the warp and weft yarns are shown at the surface twice one after the other. This is the optimal fabric weave structure to maximize one-sided illumination using cladding-removed POF. Figure 18(a)

shows the frontal face, while Figure 18(b) shows the back face on which little light is observed.

6. Conclusions

“Light” was proposed as a new tool for information delivery in wearable computers. To maximize the light-scattering amount in one direction of the fabric, the cladding of a POF was partially removed both chemically and

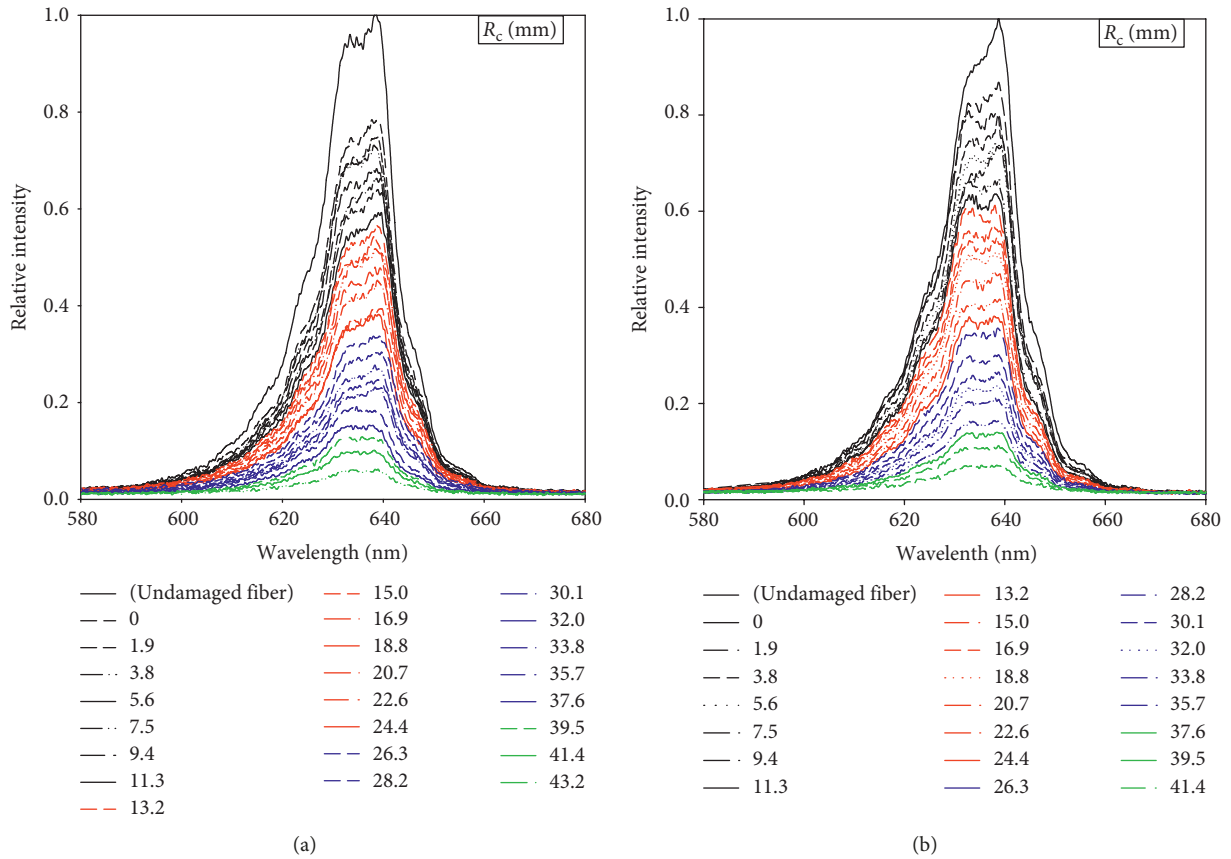


FIGURE 11: End-tip-illumination using two types of cladding removal for PGR-FB250 fiber with different cut areas. (a) Whole-cut [1]. (b) One-sided removal.

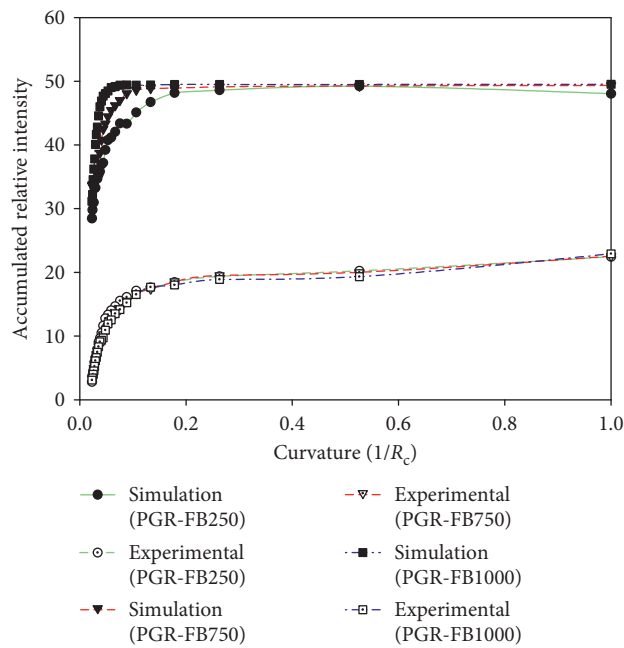


FIGURE 12: Experimental and theoretical end-tip-illumination measurement for one-sided POF using large-step simulation.

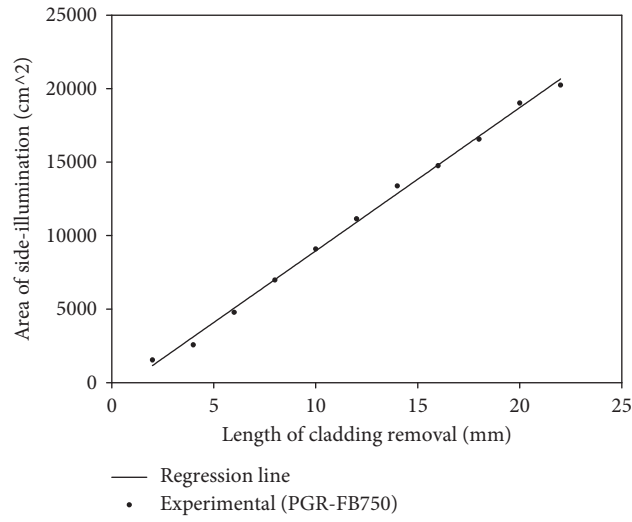


FIGURE 13: Effect of cladding removal length for uncrimped POF.

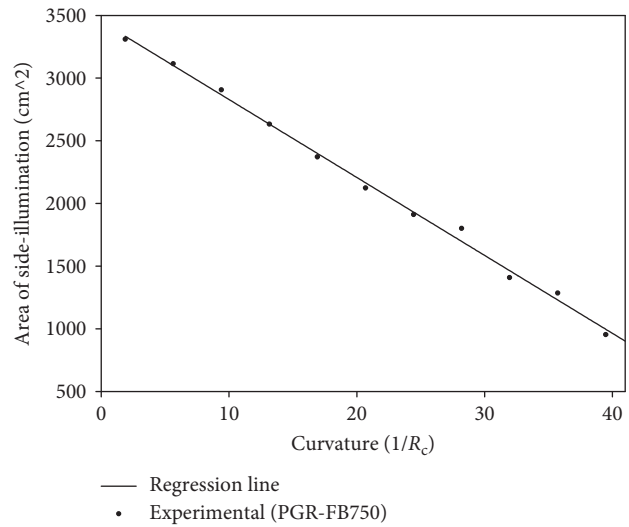


FIGURE 14: Effect of curvature on single POF side-illumination area.

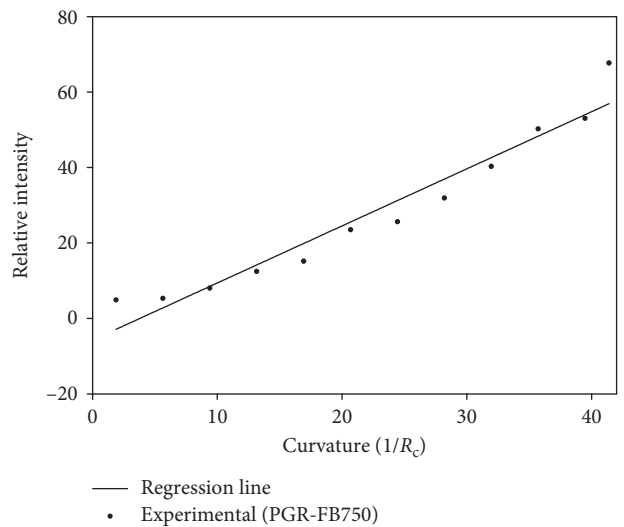


FIGURE 15: Effect of curvature on single POF side-illumination relative intensity.

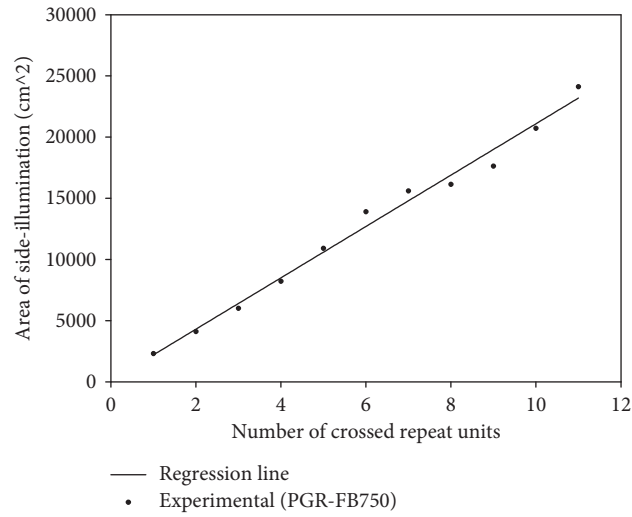


FIGURE 16: Comparison of area of side-illumination according to number of crossed repeat units.

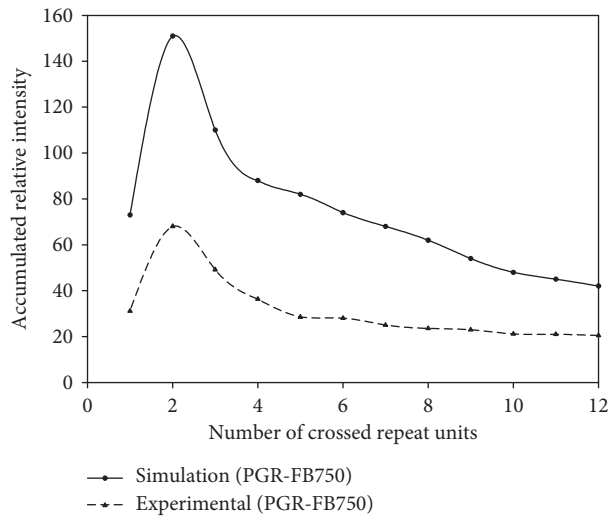


FIGURE 17: Comparison of simulation and experiment for side-illumination according to number of crossed repeat units.

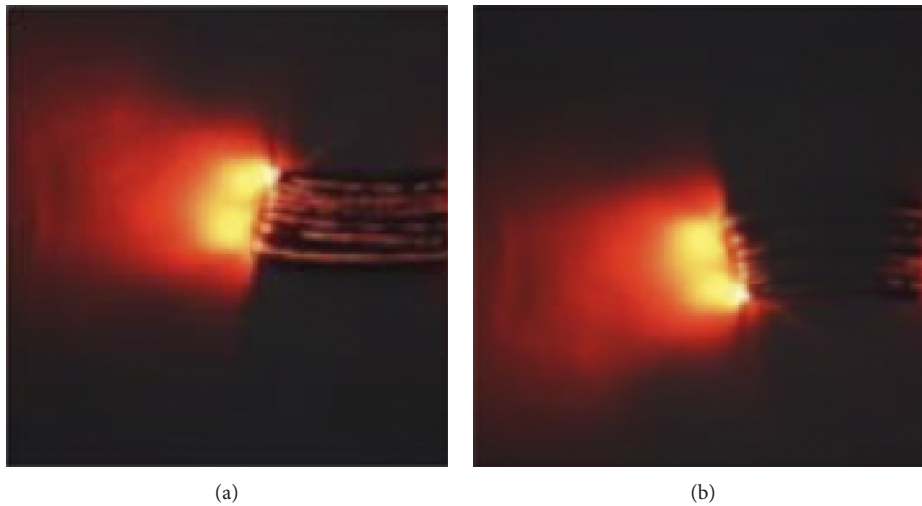


FIGURE 18: Example of a 2 by 2 twill weave fabric with one-sided cladding-removal POFs. (a) Front. (b) Back.

mechanically. The delivered light was measured quantitatively using a spectrometer at the fiber end tip and at the cladding-removed surface. One-sided cladding removal generated a more regular tendency of light scattering. The effect of cladding length, curvature, and weave pattern was also examined for a POF with crimp and without crimp. By varying the fabric weave repeat number, we found that two times of warp repeat was the optimal structure for side-illumination. The reason was thought to be a compromising effect between curvature and global bending. Moreover, the simulation technique was improved from our previous work [1]. The POF was modeled as a series of cylinders, and their coordinates were controlled by FFD and NURBS. Arbitrary weave structure could be simulated easily by inputting peg strings. The ray vectors' route was modeled by a repetitive collision detection-based algorithm and a large time step. The simulation and experimental results were very similar for POFs within the weave structure. Our ray-tracing-based simulation technique can be used for any problems with complex boundary conditions rapidly. Our further work aims to extend this research to a garment-based visible light communication system or Li-Fi [16].

Data Availability

The datasets generated during and/or analyzed during the current study are not publicly available due to domestic patent submission but are available from the corresponding author on reasonable request.

Conflicts of Interest

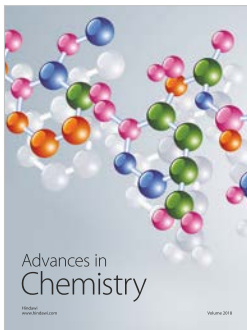
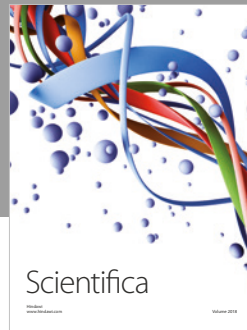
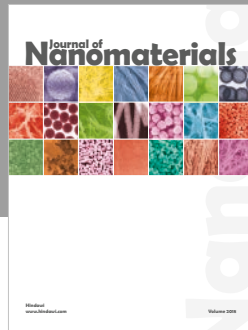
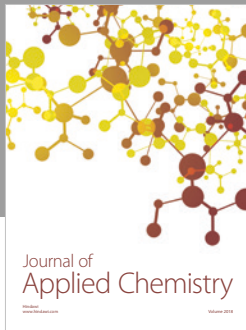
The authors declare that there are no conflicts of interest regarding the publication of this paper.

Acknowledgments

This research was supported by Kumoh National Institute of Technology (2018-104-058).

References

- [1] S. H. Moon, J. S. Lee, and I. H. Sul, "Ray-tracing-based modeling of clad-removed step-index plastic optical fiber in smart textiles: effect of curvature in plain weave fabric," *Advances in Materials Science and Engineering*, vol. 2018, Article ID 1672369, 16 pages, 2018.
- [2] A. Pantelopoulos and N. G. Bourbakis, "A survey on wearable sensor-based systems for health monitoring and prognosis," *IEEE Transactions on Systems, Man, and Cybernetics, Part C (Applications and Reviews)*, vol. 40, no. 1, pp. 1–12, 2010.
- [3] M. Stoppa and A. Chiolerio, "Wearable electronics and smart textiles: a critical review," *Sensors*, vol. 14, no. 7, pp. 11957–11992, 2014.
- [4] M. Swan, "Sensor mania! the internet of things, wearable computing, objective metrics, and the quantified self 2.0," *Journal of Sensor and Actuator Networks*, vol. 1, no. 3, pp. 217–253, 2012.
- [5] L. M. Castano and A. B. Flatau, "Smart fabric sensors and e-textile technologies: a review," *Smart Materials and Structures*, vol. 23, no. 5, article 053001, 2014.
- [6] J. Lee, H. Kwon, J. Seo et al., "Conductive fiber-based ultrasensitive textile pressure sensor for wearable electronics," *Advanced Materials*, vol. 27, no. 15, pp. 2433–2439, 2015.
- [7] K. H. Hong, K. W. Oh, and T. J. Kang, "Preparation of conducting nylon-6 electrospun fiber webs by the in situ polymerization of polyaniline," *Journal of Applied Polymer Science*, vol. 96, no. 4, pp. 983–991, 2005.
- [8] M. F. De Volder, S. H. Tawfick, R. H. Baughman, and A. J. Hart, "Carbon nanotubes: present and future commercial applications," *Science*, vol. 339, no. 6119, pp. 535–539, 2013.
- [9] W. Zeng, L. Shu, Q. Li, S. Chen, F. Wang, and X.-M. Tao, "Fiber-based wearable electronics: a review of materials, fabrication, devices, and applications," *Advanced Materials*, vol. 26, no. 31, pp. 5310–5336, 2014.
- [10] C. F. Dalziel, "Electric shock hazard," *IEEE spectrum*, vol. 9, no. 2, pp. 41–50, 1972.
- [11] J. Hecht, *City of Light: The Story of Fiber Optics*, Oxford University Press on Demand, New York, NY, USA, 2004.
- [12] S. J. Park, C.-H. Lee, K.-T. Jeong, H.-J. Park, J.-G. Ahn, and K.-H. Song, "Fiber-to-the-home services based on wavelength-division-multiplexing passive optical network," *Journal of Lightwave Technology*, vol. 22, no. 11, pp. 2582–2591, 2004.
- [13] J. Hecht, *Understanding Fiber Optics*, Laser Light Press, Auburndale, MA, USA, 2015.
- [14] Y. Fernaeus, M. Jonsson, and J. Tholander, "Revisiting the jacquard loom: threads of history and current patterns in HCI," in *Proceedings of SIGCHI Conference on Human Factors in Computing Systems*. ACM, Austin, TX, USA, May 2012.
- [15] F. T. Peirce, "5—the geometry of cloth structure," *Journal of the Textile Institute Transactions*, vol. 28, no. 3, pp. T45–T96, 1937.
- [16] D. Tsonev, S. Videv, and H. Haas, "Light fidelity (Li-Fi): towards all-optical networking," in *Broadband Access Communication Technologies VIII*, International Society for Optics and Photonics, Bellingham, WA, USA, 2014.



Hindawi
Submit your manuscripts at
www.hindawi.com

